Author: Mohammad Dehnavi **Advisor: Prof. Dr. Selçuk Yerci**

Address: Üniversiteler Mah. Dumlupınar Bul. No:1 06800, Çankaya / Ankara

Affiliation: EmPV – ODTÜ GÜNAM

Email: Mohammaddehnaviedu@gmail.com

ORCID: 0009-0006-7331-9399

Main Text paragraph about how the simulation was carried out:

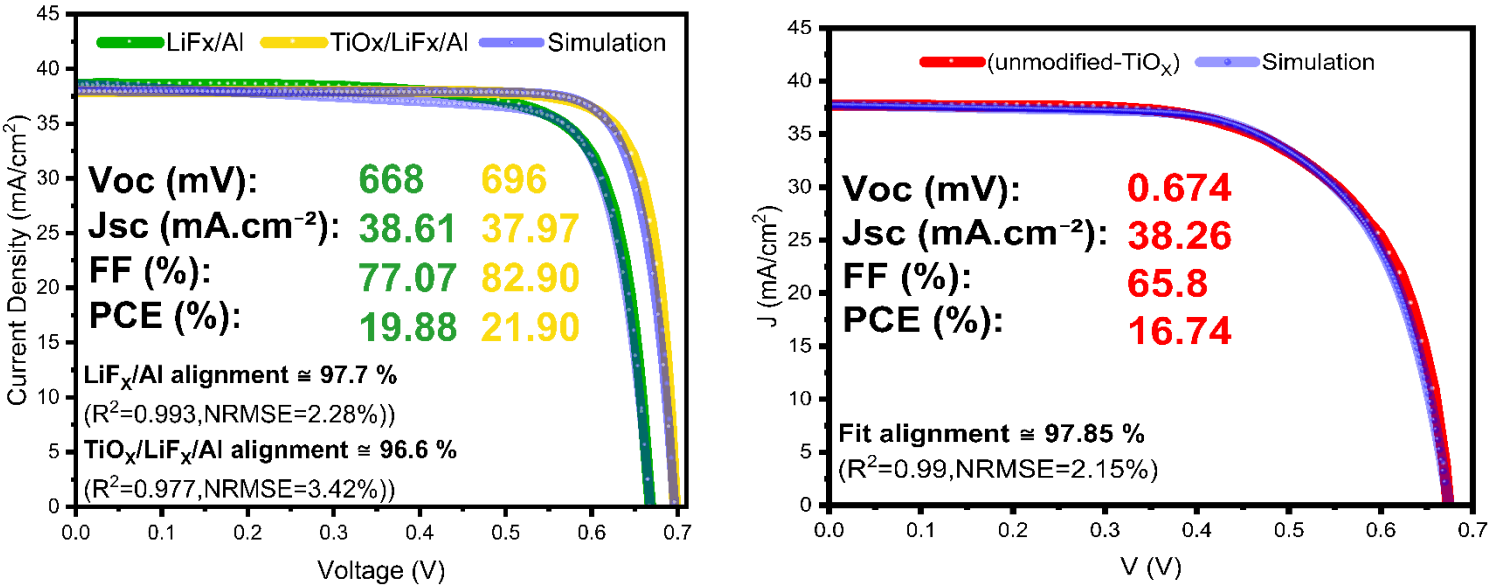

(Fig 5b, Experimental and simulation J-V curves of champion devices)

Using the experimentally measured J-V metrics and characteristics, we numerically modelled three different discussed devices with the main focus on rear-contact structures: liF/Al (no TiOx), unmodified TiOx, and modified TiOx using Solar Cell Capacitance Simulator(SCAPS)[2,3]. As for the starting point, we used a set of material and interface parameters taken from literature or directly measured quantities (e.g. thickness, Bandgap) and then varied them within physically acceptable ranges until J-V metrics(Voc,Jsc,FF) and its overall shape of simulated curves closely matched those of the corresponding champion devices. Once a consistent parameter set was obtained for each structure, we further adjusted the parameters so that the simulations reproduced the average J-V metrics of all devices of that structure, ensuring that the final models represent a typical device rather than isolated best cells. All reported results in this work correspond to a typical device of each structure that form a basis for the quantitative analysis presented.

Q3: “The UPS data shows a WF reduction, which is attributed to charge transfer doping from the Ti-OO complex. However, this interpretation is speculative without direct evidence of the electronic density of states (DOS) near the conduction band. Direct and quantitative methods like electron energy loss spectroscopy (EELS), would be highly valuable to confirm the proposed introduction of donor states.”

To interpret the UPS outcome on reduction of work-function (≈4.9 → 4.3 eV) within SCAPS, we represent the additional donor-like density of states introduced by Ti–OO complexes as a shallow donor-type interface defect at the c-Si/TiO_x rear interface, located 0.1 eV below the conduction band edge. This modelling of charge-transfer doping and fixed positive charge as shallow donor-type interface states is consistent with general methodology discussed by Burgelman *et al for SCAPS*. [3] Provided in table 3, to ensure that these states act predominantly as electron donors/selective states rather than as recombination centers, we assign them an electron capture cross section of 1×10^{-15} and a much smaller hole capture cross section of 1×10^{-22} discussed in more details in previous studies. [16,17,18]

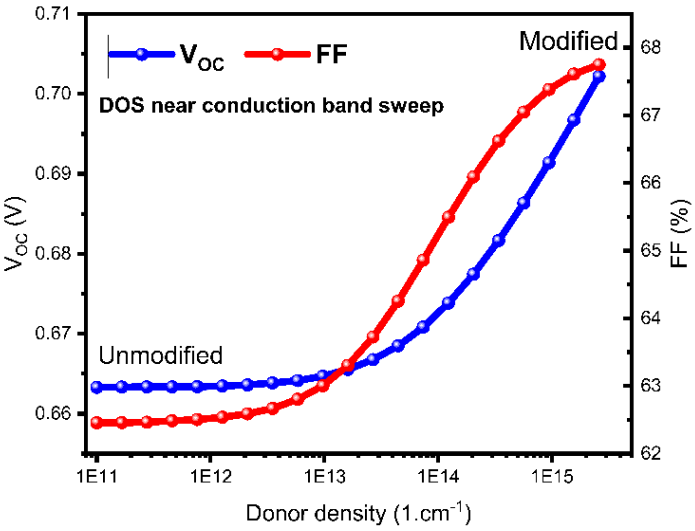

Figure 1 (DOS near CB sweep from unmodified value to the modified value to demonstrate the isolated effect of this parameter)

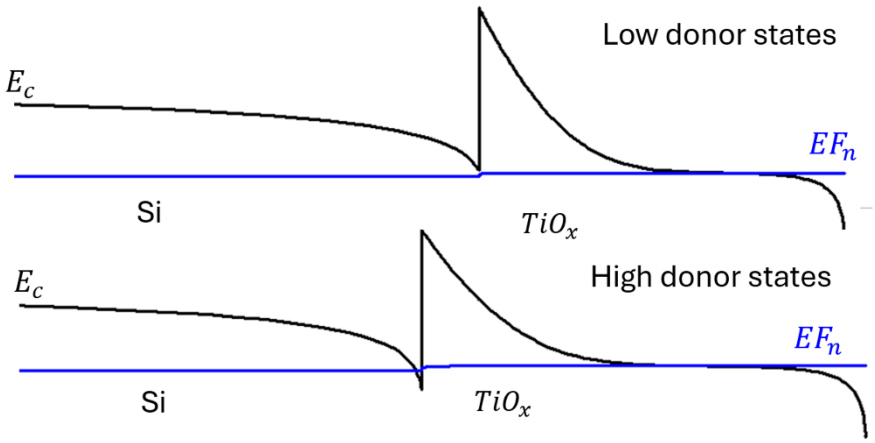

Figure 2 (Rear interface band diagram of unmodified TiOx before and after increasing donor density obtained under dark in SCAPS)

As to isolate the effect of the donor DOS, all device parameters were fixed to those of the unmodified TiO_x and only the donor interface density D_{it_donor} was swept from that of unmodified to the modified value (1×10^{11} → 2.6×10^{15}) illustrated in figure 1. The map in this figure shows that above ~10^{13} density values both Voc/FF increase notably.

Supporting this trend, the band diagrams in figures 2 show that solely increasing donor density causes a slightly stronger bending of conduction band at the Si/TiOx interface and brings it slightly below the electron quasi-Fermi level EF_n, consistent with strong electron accumulation near E_c due to positively charged donor states. In conclusion, a rise in DOS near conduction band is sufficient on its own to result in a simultaneous gain in both metrics in an otherwise unchanged device, in line with the UPS based picture of additional donor states introduced upon modification.

This approach does not replace a direct DOS measurement such as EELS, but it shows that the magnitude of donor DOS required to explain the UPS work function shift is quantitatively consistent with the observed Voc/FF trends, supporting the proposed donor-state near E_c interpretation.

On the other hand, a deep neutral defect was included to represent recombination active interface traps in the mid-gap at 0.6 eV above the valence band. The density of this defect is rather higher in the unmodified device which will be strongly reduced as we go toward the modified structure resulting in a cleaner interface.

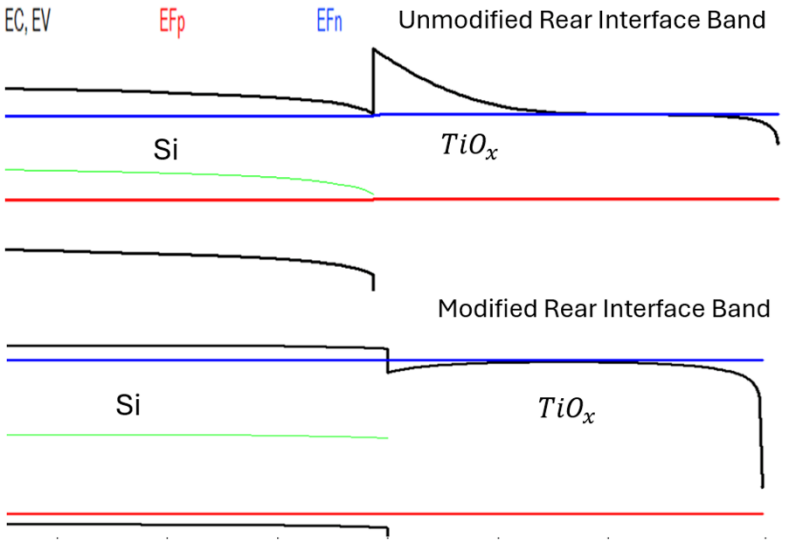

Figure 3 (Band diagrams of the unmodified and modified devices under dark)

The band diagrams at the rear contact for the unmodified and modified TiO_x devices (Fig3) further support this interpretation. In the unmodified case, the c-Si conduction band bends downward as the interface is approached and the conduction band in TiO_x forms a considerable spike above the electron quasi-Fermi level EF_n. This reflects a combination of strong Fermi-level pinning by the high mid-gap interface trap density and the lower effective electron affinity of the unmodified TiO_x, and corresponds to a barrier for electron extraction. In the modified structure, the reduced mid-gap Dit together with the higher electron affinity and the additional shallow donor-like states near E_c pull the TiO_x conduction band closer to E_{Fn}. In the band diagram, the TiO conduction band at the Si/TiO_x interface steps slightly below EF_n and then runs almost parallel to it inside the oxide before bending toward the metal contact. This corresponds to an electron-selective, low-barrier contact: majority electrons see an energetically favorable path into the rear contact,

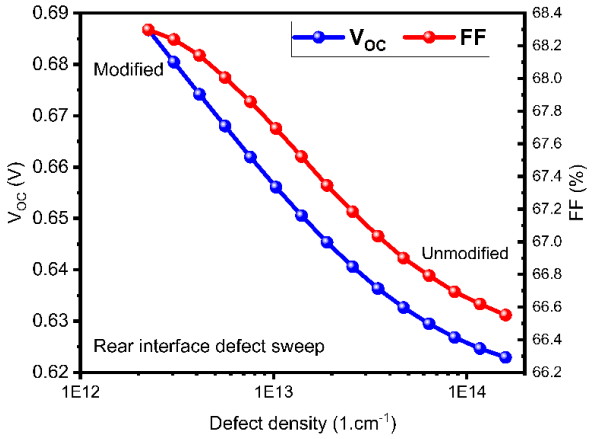

Figure 4 (Rear interface defect density sweep from unmodified to modified and its effect on Voc and FF)

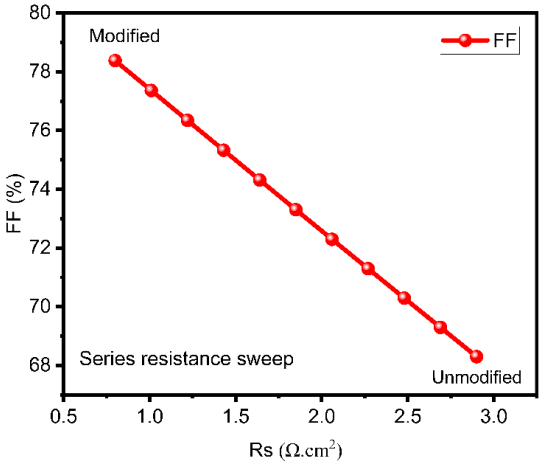

Figure 5 (Effect of independently increasing series resistance on fill factor)

while minority holes face a large valence-band offset at the Si/TiO_x interface and are effectively blocked. Taken together, the removal of the E_c spike, the strong reduction of deep mid-gap Dit, and the higher density of shallow donor-like states near E_c reduce the effective interface recombination and contact resistance at the rear contact and thereby account for the portion of the measured increase in both Voc and FF when going from the unmodified to the modified TiO_x contact.

After concluding that increasing the donor-like DOS near the conduction band (from the unmodified value 1×10^{11} to 2.6×10^{15} cm^{-2}) already gives a simultaneous rise in Voc and FF (Fig. 1), we next quantified the impact of the remaining parameters. Once the donor DOS and corresponding TiOx affinity were set to their modified values, all other quantities were frozen, and we swept only the rear-interface defect density D_{it_neutral} from the high value of the unmodified contact down to the low value of the modified one (Fig. 4). This sweep suggests that both Voc and FF improve monotonically, showing that the reduction of recombination-active mid-gap Dit provides an additional gain beyond that from donor DOS alone. Finally, with the interface properties fixed, we varied only the series resistance from the lower value used for the modified device to the higher value of the unmodified contact (Fig. 5); as expected, FF degrades almost linearly with increasing R_s while Voc remains nearly unchanged, confirming that the remaining FF difference between the two structures is dominated by resistive losses at the rear contact.

Overall, the combined band-diagram analysis and targeted parameter sweeps provide a quantitative explanation of how the added donor-like states, reduced mid-gap Dit, and improved rear contact jointly drive the performance changes from the unmodified to the modified TiOx device.

Q6: “Device Performance and Fill Factor (FF): The significant improvement in FF (from 77.07% to 82.9%) is a key result. The authors' explanation, linking it to reduced recombination, is plausible but insufficient.”

Building on the unmodified/modified TiO_x analysis, when reproducing the reference LiF/Al and modified $TiO_x/LiF/Al$ devices in SCAPS (for both champion and a typical device), all silicon and front-contact parameters were kept identical; only the rear region was changed by adding the TiO_x layer, its associated rear-interface defects, and the corresponding shift in rear-contact work function.

Overall, the modified device is characterized by three main factors: (i) a higher donor-like DOS close to E_c, (ii) a reduced deep mid-gap defect density at the rear interface, and (iii) improved series and shunt resistances

As summarized in the SI tables, the modified device differs from the LiF/Al reference mainly by (i) a larger effective electron affinity of the rear layer, (ii) addition of shallow donor-like states with a high density close to E_c (iii) a much lower density of deep mid-gap interface defects, and (iv) improved series and shunt resistances extracted from fitting J–V curves and metrics.

The higher χ together with the donor-like DOS shifts the TiO_x conduction band closer to the electron quasi-Fermi level at the rear interface, creating an electron-accumulating, hole-blocking contact, while the wide TiO_x band gap keeps the valence band far from EF_n. Together, these changes lower the effective rear J_0 and recombination, while simultaneously reducing resistive losses Consequently, the higher V_{oc} and FF of the $TiO_x/LiF/Al$ device can be attributed to the combined effect of improved band alignment (via higher χ), increased donor DOS near the conduction band, lower recombination-active Dit, and better R_s/R_{sh} at the rear contact.

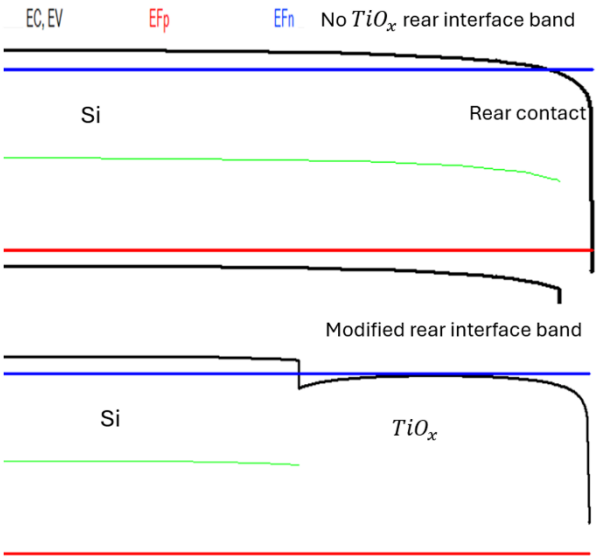

Figure 6 (Band diagrams of the unmodified and modified devices under dark)

Supplementary Information:

SCAPS reproducibility:

Table 1: Global SCAPS settings and contacts

Geometry, Scan, Illumination	
Illumination	From left (front contact), AM1.5G, 1 sun, 300K. [1,2]
Series / Shunt $\Omega \cdot cm^2$	R_s = Variable ; $R_{sh} = Variable.$
Contact optical filters	Transmission values: $T_{no\ TiOx}$= 0.854, $T_{unmodified}$= 0.884, $T_{modified}$= 0.863, (used as a flat front-side loss proxy). [4]
Scaps contact mapping	
Left contact (front)	Ag/Al_2O_3/SiNx ; Flatband. [2,3]
SRVs ($cm.s^{-1}$)	$S_n = 1 \times 10^3$, $S_p = 1 \times 10^7$ [2,5]
Right contact (Rear)	Al; Work function $\Phi = 4.3\ eV$ [6]. $\Phi_{eff\ TiOx} = 3.4$ $\Phi_{eff\ no\ TiOx} = 3$ *
SRVs ($cm.s^{-1}$)	$S_n = 1 \times 10^7$, $S_p = 1 \times 10^3$ [2,5]

Note: "variable" indicates composition-dependent values reported in table 4.

*: Effective work functions were chosen to take the effect of LiF and TiOx on the rear contact into account.

Table2: Layer parameters

Layer / **parameter**	**P^+ c-Si** (emitter)	**n c-Si** (bulk)	**TiO_x** (Unmodified)	**TiO_x** (Modified)	**LiF**{II}
Thickness (μm)	0.1	140	0.01	0.017	0.001
Bandgap E_g (eV)	1.12	1.12	3.65	3.73	10
Electron affinity χ (eV)	4.05	4.05	3.6 {I}	4.2	$\chi_{above\ layer}$
Dielectric permittivity ε_r	11.7	11.7	10	10	10
Density of states (cm^{-3})	$N_C = 2.8 \times 10^{19}$ $N_V = 1 \times 10^{19}$	$N_C = 2.8 \times 10^{19}$ $N_V = 1 \times 10^{19}$	$N_C = 1 \times 10^{18}$ $N_V = 1 \times 10^{18}$	$N_C = 1 \times 10^{18}$ $N_V = 1 \times 10^{18}$	$N_C = 1 \times 10^{20}$ $N_V = 1 \times 10^{20}$
Thermal velocities v_{th} $(cm.s^{-1})$	1×10^7 (n, p)	1×10^7 (n, p)	1×10^7 (n, p)	1×10^7 (n, p)	1×10^7 (n, p)
Mobilities $(\text{cm}^2.\text{V}^{-1}.\text{s}^{-1})$	$\mu_n = 1200$ $\mu_p = 500$	$\mu_n = 1250$ $\mu_p = 500$	$\mu_n = 25$ $\mu_p = 10$	$\mu_n = 25$ $\mu_p = 10$	$\mu_n = 1$ $\mu_p = 1$
Doping (cm^{-3})	$N_A = 1 \times 10^{19}$ $N_D = 0$	$N_A = 0$ $N_D = 4 \times 10^{15}$	$N_A = 0$ $N_D = 1 \times 10^{18}$	$N_A = 0$ $N_D = 1 \times 10^{18}$	$N_A = 0$ $N_D = 1 \times 10^7$
Bulk SRH density of recombination: N_t (cm^{-3})	1×10^{12}	5.3×10^{11}	none	none	none
Bulk SRH cross sections: σ_n, σ_p (cm^2)	$\sigma_n = 1 \times 10^{-15}$ $\sigma_p = 1 \times 10^{-15}$	$\sigma_n = 1 \times 10^{-15}$ $\sigma_p = 1 \times 10^{-15}$	none	none	none
Bulk SRH defect energy level: E_t (eV)	0.56 above E_V	0.56 above E_V	none	none	none
Reference(s)	[7,8,9]	[8,10,11,12]	[13,14,20,21]	[13,14]	[15]

{I}: We use the relation $\varphi = \chi + E_g - (E_f - E_v)$ between the UPS wok function (φ), electron affinity (χ), and band edges. Inserting the UPS values $\varphi_{unmod} = 4.9$, $\varphi_{mod} = 4.3$, $Eg_{unmod} = 3.65$, $Eg_{mod} = 3.73$ and $E_f - E_v = 3.7$ would

result in electron affinities significantly larger than typical reported values for TiO_x and would not lead to physically realistic band alignment when applied in SCAPS. In addition, UPS measures the free surface of a thick TiO_x film in vacuum while χ in SCAPS acts as an effective parameter for c-Si/TiOx interface. This effective parameter accounts for interface dipoles and local DOS, which can shift band edges differently than the vacuum level. For this reason, we do not enforce a one-to-one inversion of the UPS data to χ in the simulations. Instead, χ is kept within a physically reasonable range consistent with prior studies [20,21] and the UPS-derived trend (lower WF and increased donor like DOS upon modification) is implemented via a combination of χ, donor-like interface states near E_c , and neutral Dit as described in the text. Therefore, χ is a fitted parameter here and not claimed physically.

{II}: To avoid convergence/calculation issues, LiF's electron affinity (χ_{LiF}) was set to that of the layer sitting above it. This layer was only modelled for fitting champion devices and then removed for typical devices for better convergence. Instead, the effect of LiF on the rear contact's work function was applied as its role is an ultrathin interfacial modifier. This does not affect the composition-dependent trends, which are mostly governed by the TiO_x and rear interface parameters.

Table 3: Interface profile

Structure	**No TiO_x**	**TiO_x** (Unmodified)		**TiO_x** (Modified)	
Rear Interface / **Parameter**	Defect 1 (Neutral)	Defect 1 (Donor)	Defect 2(Neutral)	Defect 1(Donor)	Defect 2(Neutral)
Energy reference E_t	single at 0.60 eV (above highest E_V)	single at 0.10 eV (below the lowest E_c)	single at 0.60 eV (above highest E_V)	single at 0.10 eV (below the lowest E_c)	single at 0.60 eV (above highest E_V)
Capture cross-sections (cm^2) [16,17,18]	$\sigma_n = 1 \times 10^{-15}$ $\sigma_p = 1 \times 10^{-15}$	$\sigma_n = 1 \times 10^{-15}$ $\sigma_p = 1 \times 10^{-22}$	$\sigma_n = 1 \times 10^{-15}$ $\sigma_p = 1 \times 10^{-15}$	$\sigma_n = 1 \times 10^{-15}$ $\sigma_p = 1 \times 10^{-22}$	$\sigma_n = 1 \times 10^{-15}$ $\sigma_p = 1 \times 10^{-15}$
Defect density D_{it} (cm^{-2}) [19]	1.62×10^{14}	1×10^{11}	1.59×10^{14}	2.6×10^{15}	2.25×10^{12}

Table 4: R_s/R_{sh} and I-V metrics for different structures.

Structure / **Parameter**	**No TiO_x**	**TiO_x** (Unmodified)	**TiO_x** (Modified)
Series resistance R_{sh} ($\Omega.cm^2$)	1.40	2.90	0.80
Shunt resistance R_{sh} ($\Omega.cm^2$)	2.5×10^3	1.0×10^3	4.0×10^3
Device metrics			
V_{oc} (V)	0.664	0.663	0.686
$J_{sc}(mA.cm^{-2})$	37.1	38.32	37.5
$FF(\%)$	75.8	62.46	79.3
$PCE(\%)$	18.6	15.88	20.4

Extra details:

Table x: Varied parameters for unmodified and modified TiO_x structures.

Structure / Parameter	TiO_x (Unmodified)	TiO_x (Modified)
Thickness (nm)	10	17
Electron affinity χ (eV)	3.6	4.2
Bandgap (eV)		
Rear interface donor density D_{it_donor} (cm^{-2})	1.0×10^{11}	2.6×10^{15}
Rear interface neutral defect $D_{it\_neutral}$ (cm^{-2})	1.59×10^{14}	2.25×10^{12}
Series resistance R_{sh} ($\Omega.cm^2$)	2.9	0.80
Shunt resistance R_{sh} ($\Omega.cm^2$)	1.0×10^3	4.0×10^3
Device metrics		
V_{oc} (V)	0.663	0.686
$J_{sc}(mA.cm^{-2})$	38.32	37.5
$FF(\%)$	62.46	79.3
$PCE(\%)$	15.88	20.4

Table x: Varied parameters for unmodified and modified TiO_x structures.

Structure / Parameter	No TiO_x (Base)	TiO_x (Modified)
Electron affinity χ (eV)	-	4.2
Rear interface donor density D_{it_donor} (cm^{-2})	-	2.6×10^{15}
Rear interface neutral defect $D_{it\_neutral}$ (cm^{-2})	1.62×10^{14}	2.25×10^{12}
Series resistance R_{sh} ($\Omega.cm^2$)	1.4	0.80
Shunt resistance R_{sh} ($\Omega.cm^2$)	2.5×10^3	4.0×10^3
Device metrics		
V_{oc} (V)	0.664	0.686
$J_{sc}(mA.cm^{-2})$	37.1	37.5
$FF(\%)$	75.8	79.3
$PCE(\%)$	18.6	20.4

1. NREL. "Reference Air Mass 1.5 Spectra." National Renewable Energy Laboratory. Available at: https://www.nrel.gov/grid/solar-resource/spectra-am1.5
2. Burgelman, M.; Decock, K.; Niemegeers, A.; Verschraegen, J.; Degrave, S. SCAPS Manual. University of Gent (ELIS), "most recent version". https://scaps.elis.ugent.be/SCAPS%20manual%20most%20recent.pdf
3. Burgelman, M., Nollet, P., & Degrave, S. (2000). Modelling polycrystalline semiconductor solar cells. *Thin Solid Films*, *361*, 527–532. https://doi.org/10.1016/S0040-6090(99)00825-1
4. Wu, D.; Jia, R.; Ding, W.; Chen, C.; Wu, D.; Chen, W.; Li, H.; Yue, H.; Liu, X. Optimization of Al_2O_3/SiN_x Stacked Antireflection Structures for N-Type Surface-Passivated Crystalline Silicon Solar Cells. J. Semicond. 2011, 32 (9), 094008. https://doi.org/10.1088/1674-4926/32/9/094008
5. Aberle, A. G. Surface passivation of crystalline silicon solar cells: a review. *Progress in Photovoltaics: Research and Applications* 8 (5), 473–487 (2000). https://doi.org/10.1002/1099-159X(200009/10)8:5<473::AID-PIP337>3.0.CO;2-D
6. Eastment, R., & Mee, C. (n.d.). *Work function measurements on (100),(110) and (111) surfaces of aluminium*. https://iopscience.iop.org/article/10.1088/0305-4608/3/9/016/meta
7. Ramli, N. F.; Sepeai, S.; Rostan, N. F. M.; Ludin, N. A.; Ibrahim, M. A.; Teridi, M. A. M.; Zaidi, S. H. Model development of monolithic tandem silicon–perovskite solar cell by SCAPS simulation. *AIP Conference Proceedings* 1838, 020006 (2017). https://doi.org/10.1063/1.4982178
8. Akoto, E.; Isahi, V.; Odari, V.; Maghanga, C.; Nyongesa, F. Monolith $Cs_{1-x}Rb_xSnI_3$ perovskite–silicon 2T tandem solar cell using SCAPS-1D. *Results in Optics* 12, 100470 (2023). https://doi.org/10.1016/j.rio.2023.100470
9. Moinuddin, R. M.; Hasan, M.; Rahaman, M.; Islam, K. S. Numerical optimization and efficiency analysis of Sn-based perovskite-on-silicon tandem solar cells with various TCO materials using SCAPS-1D simulation. *AIP Advances* 14, 085126 (2024). https://doi.org/10.1063/5.0217477
10. Rahmouni, M.; Datta, A.; Chatterjee, P.; Damon-Lacoste, J.; Ballif, C.; Roca i Cabarrocas, P. *Carrier transport and sensitivity issues in heterojunction with intrinsic thin layer solar cells on N-type crystalline silicon: A computer simulation study.* Journal of Applied Physics 107 (5), 054521 (2010). https://doi.org/10.1063/1.3326945
11. Richter, A.; Werner, F.; Cuevas, A.; Schmidt, J.; Glunz, S. W. *Improved parameterization of Auger recombination in silicon.* Energy Procedia 27, 88–94 (2012). https://doi.org/10.1016/j.egypro.2012.07.034
12. Li, S. S.; Thurber, W. R. *The dopant density and temperature dependence of electron mobility and resistivity in n-type silicon.* Solid-State Electronics 20 (7), 609–616 (1977). https://doi.org/10.1016/0038-1101(77)90100-9
13. Pochont, N. R.; Sekhar, Y. R.; Vasu, K.; Jose, R. *Nitrogen-Doped Titanium Dioxide as a Hole Transport Layer for High-Efficiency Formamidinium Perovskite Solar Cells.* Molecules 27, 7927 (2022). https://doi.org/10.3390/molecules27227927
14. Usman, A.; Bovornratanaraks, T. *Modeling and Optimization of Modified TiO_2 with Aluminum and Magnesium as ETL in $MAPbI_3$ Perovskite Solar Cells: SCAPS 1D Frameworks.* ACS Omega 9, 39663–39672 (2024). https://doi.org/10.1021/acsomega.4c04505
15. Khokhar, M. Q.; Hussain, S. Q.; Pham, D. P.; Lee, S.; Park, H.; Kim, Y.; Cho, E.; Yi, J. *Simulation of Silicon Heterojunction Solar Cells for High Efficiency with Lithium Fluoride Electron Carrier Selective Layer.* Energies 2020, 13 (7), 1635. https://doi.org/10.3390/en13071635
16. Hu, C.-M., and W. G. Oldham, "Carrier recombination through donors/acceptors in heavily doped silicon," *Applied Physics Letters*, 35(8), 636–639 (1979). https://doi.org/10.1063/1.91234

17. Geerligs, L. J., D. Macdonald, and G. Coletti, "Possible reduction of recombination lifetime due to compensated dopants," *17th Workshop on Crystalline Silicon Solar Cells & Modules: Materials and Processes*, Vail, CO, USA, 5–8 Aug. 2007. https://resolver.tno.nl/uuid:69893a3d-cdd6-49ac-9e1c-d959a71739e6.
18. Ryan et al. (huge spread of interface-state capture cross sections)
Ryan, J. T.; Matsuda, A.; Campbell, J. P.; Cheung, K. P. *Interface-state capture cross section—Why does it vary so much?* Applied Physics Letters 106, 163503 (2015). https://doi.org/10.1063/1.4919100
19. Haque, M. M.; Mahjabin, S.; Nizam, U.; Al Reza, A.; Alam, M. Z.; Amin, N.; Sopian, K.; Karim, M. R. Study on the interface defects of eco-friendly perovskite solar cells. *Solar Energy* 247, 96–108 (2022). https://doi.org/10.1016/j.solener.2022.10.024
20. Osterthun, M.; Wietler, T. F.; Oh, J.; Kuck, D.; Hensel, T.; Lackner, D.; Höhn, O.; Dimroth, F.; Olk, D. *Titanium-Oxide-Based Electron-Selective Contact for Ultrathin Germanium Quantum Well Solar Cell.* Phys. Status Solidi A 2022, *219*, 2200292. https://doi.org/10.1002/pssa.202200292

21. Tekin, S. B.; Demirci, K. Y.; Güneş, S. *Electron Affinity of Metal Oxide Thin Films of TiO_2, ZnO, and NiO and Their Applicability in 28.3 THz Rectenna Devices.* J. Appl. Phys. 2023, *134*, 084503. https://doi.org/10.1063/5.0157726